Extended Rotational Coherence of Polar Molecules in an Elliptically Polarized Trap

Annie J. Park, Lewis R. B. Picard, Gabriel E. Patenotte, Jessie T. Zhang, Till Rosenband, and Kang-Kuen Ni

Extended rotational coherence of polar molecules in an elliptically polarized trap

Annie J. Park,[1, 2, 3, *] Lewis R.B. Picard,[2, 1, 3, *] Gabriel E. Patenotte,[2, 1, 3]
Jessie T. Zhang,[1, 2, 3, †] Till Rosenband,[4] and Kang-Kuen Ni[1, 2, 3, ‡]

[1]*Department of Chemistry and Chemical Biology, Harvard University, Cambridge, Massachusetts 02138, USA*
[2]*Department of Physics, Harvard University, Cambridge, Massachusetts 02138, USA*
[3]*Harvard-MIT Center for Ultracold Atoms, Cambridge, Massachusetts 02138, USA*
[4]*Agendile LLC, Cambridge, Massachusetts, 02140, USA*
(Dated: October 4, 2023)

We demonstrate long rotational coherence of individual polar molecules in the motional ground state of an optical trap. In the present, previously unexplored regime, the rotational eigenstates of molecules are dominantly quantized by trapping light rather than static fields, and the main source of decoherence is differential light shift. In an optical tweezer array of NaCs molecules, we achieve a three-orders-of-magnitude reduction in differential light shift by changing the trap's polarization from linear to a specific "magic" ellipticity. With spin-echo pulses, we measure a rotational coherence time of 62(3) ms (one pulse) and 250(40) ms (up to 72 pulses), surpassing the projected duration of resonant dipole-dipole entangling gates by orders of magnitude.

Protecting quantum systems from decoherence is necessary for quantum metrology, simulation, and information processing. Polar molecules are promising building blocks for these applications due to their rich identical structure, long coherence times [1–4], and intrinsic anisotropic electric dipole-dipole interactions [5, 6]. Crucially, dipole-dipole interactions can deterministically entangle two rotation states of spatially separated molecules [7, 8], as demonstrated recently with CaF molecules in optical tweezers [9, 10]. In such a case, where the molecules are directly laser cooled and loaded into optical tweezers, the fidelity of entanglement has been limited by residual thermal motion, which causes uncontrolled variation in the strength of entangling interactions.

This limit can be overcome by using molecules prepared in the lowest motional state of an optical tweezer. For bi-alkali molecules associated from laser-cooled atoms, a predominant three-dimensional motional ground state population is inherited from the association process [11–13]. The dominant source of decoherence is then due to the optical trap that spatially confines the molecules. The anisotropic polarizability of different rotational wavefunctions induces state dependent trap depths, leading to fluctuating transition frequencies and the dephasing of rotation states [14]. Therefore, canceling differential light shifts is a major hurdle that must be overcome to achieve quantum coherence with these species as they undergo dipolar interactions.

Many approaches have been developed to reduce the differential light shift between rotational ground ($N = 0$) and excited ($N \geq 1$) states. These approaches include selecting a specific angle between the confining light's linear polarization and static magnetic or electric fields [14–17], using a particular trapping wavelength [18–20] or intensity [21], or a specific magnetic field [6]. In the first approach, the static field determines the orientation of the excited rotational eigenstates, and a specific polar-

ization angle matches the polarizability of one excited state to the ground state. This method, however, is not applicable even at moderate trap depths when the differential light shifts are of similar magnitude to the shifts induced by the static fields, such as for polar molecules confined in optical tweezers (Fig. 1 (a)). In this deep trap regime, the rotational eigenstates are determined by the polarization of the tweezer light, rather than an external static field. For open-shell ground-state $X^2\Sigma^+$ molecules such as CaF, an isotropic $F = 0$ state within the $N = 1$ manifold is available that eliminates the first-order differential light shift [2], enabling observation of dipolar interactions [9, 10]. However, for other choices of state pairs, including those with the largest transition dipole moments, a large first-order differential light shift is expected.

In this Letter, we employ a method to trap $X^1\Sigma^+$ NaCs molecules in optical tweezers with "magic" elliptical polarization, to reduce the differential light shift by more than three orders of magnitude. Here, "magic" refers to a specific degree of ellipticity near $\chi_\mathrm{m} = \frac{1}{2}\cos^{-1}(1/3) \approx 35.26°$ that nulls the differential light shift [22]. Similar methods have been explored in atomic systems [23–26]. We measure the reduction of differential shift by microwave spectroscopy and use Ramsey interferometry to characterize the coherence. With the aid of dynamical decoupling pulses, we achieve a coherence time of 250(40) ms.

Some theoretical aspects of "magic" ellipticity trapping have been described in Ref. [22]. The ground state of rotation ($N = 0$) is illustrated in Fig. 1 (a) as a spherically symmetric rotational wavefunction with isotropic polarizability $(2\alpha_\perp + \alpha_{||})/3$ for any optical polarization, where $(\alpha_{||})$ and $(\alpha_\perp)$ are the molecule's parallel and perpendicular polarizability with respect to the internuclear axis. This approximation is valid when the trap depth is small compared to the energy of $N = 2$ excited states (the optical potential couples states with both $\Delta N = 0$ and
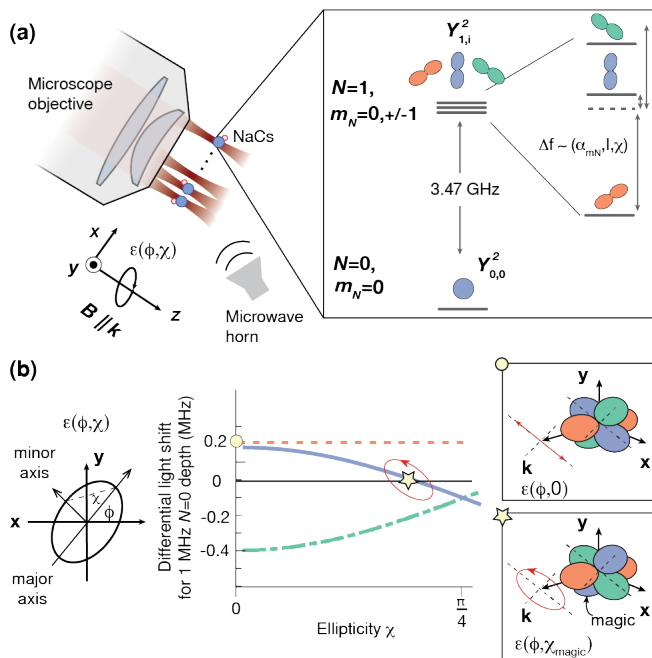
FIG. 1. NaCs molecules trapped in an optical tweezer array. (a) Schematic of the experimental setup, including the tweezer $\boldsymbol{k}$-vector, magnetic field $\boldsymbol{B}$, and trap polarization $\boldsymbol{\epsilon}(\phi, \chi)$. On the right is a simplified energy level diagram of ground ($N = 0$) and first excited ($N = 1$) rotational states, where the optical trap lifts the sublevel degeneracy. (b) The azimuthal angle ϕ and ellipticity χ of polarization determine the orientation and light shift respectively of the $N = 1$ sublevels. Unlike for linear polarization (circle), at the magic ellipticity χ_m (star), the differential light shift with respect to $N = 0$ is zero for one $N = 1$ sublevel.

$\Delta N = 2$) [27]. Throughout the text, *trap depth* (U) refers to the optical potential experienced by the relatively unperturbed $N = 0$ state. This spectroscopic study uses frequency units that are implicitly related to energy by Planck's constant.

As shown in Fig. 1 (b), for $N = 1$ the trap-induced light shift lifts the degeneracy of the three rotational sublevels ($m_N = -1, 0, 1$), and strongly perturbs their wavefunctions, such that each sublevel has well-defined orientation relative to the optical polarization above a certain trap depth threshold. This threshold is relatively low for NaCs due to its molecule hyperfine structure, small Zeeman interaction, and anisotropy of polarization. At a magnetic field of 864.5 Gauss, a value relevant for our work, the p-orbital of the lowest eigenstate dominantly aligns with the trap's polarization at a trap depth of around 100 kHz (>99.5 overlap with the $p-$orbital aligned along the trap's polarization). In a linearly polarized trap the light shift is as large as 400.8 kHz/(MHz trap depth), or a ratio to trap depth of 0.4. By tuning the ellipticity [28] near χ_m, we can eliminate this differential light shift to first order.

We implement the magic ellipticity trapping scheme

with an array of individual NaCs molecules in optical tweezers prepared using methods and an apparatus described previously [12, 29], with minor modifications described here. In brief, we first load parallel tweezer arrays of individual Na and Cs atoms. The wavelengths of the trapping lasers are 616 nm for Na and 1064 nm and for Cs, and the spacing between neighboring traps is $\sim$5 μm.

The stochastically loaded atoms are then rearranged to a densely filled array of 8 traps for each species [30, 31]. After motional ground state cooling and state preparation [32, 33], the Na atoms are adiabatically transported into the 1064 nm traps, and the atom pairs are converted into weakly bound molecules by sweeping the magnetic field across a Feshbach resonance [29] before holding at 864.5 Gauss. Subsequently, molecules are coherently transferred to their $X^1\Sigma^+$ rovibronic ground state with hyperfine quantum numbers $|I_{Na}, M_{Na}, I_{Cs}, M_{Cs}\rangle = |3/2, 3/2, 7/2, 5/2\rangle$ via stimulated Raman adiabatic passage [34] and predominately occupy the motional ground state of the traps [35]. After molecule creation, we apply a pulse resonant with the Cs D_2 transition to blast away any residual atoms. To detect molecules, we reverse the steps and image the atoms. The Cs blast step provides a background free molecule signal.

Because atomic state preparation, cooling, and detection require linearly polarized tweezer light, it is necessary to change the polarization from linear to elliptical and back during the experiment sequence. For this purpose, a motorized stage (Griffin Motion, RTS100) rotates a quarter-wave plate (QWP) by χ_m in about 100 ms with a repeatability of $\pm 0.0007°$. To ensure polarization purity and minimize site-to-site polarization variation across the array, we use a Glan-Taylor polarizer and place the QWP as the last element before the microscope objective. Before the QWP, the polarization extinction ratio is approximately 300,000.

To characterize differential light shifts under various trap polarizations and intensities, we perform rotational microwave spectroscopy to selectively transfer the molecules from $N = 0$ to the relevant $N = 1$ sublevel with a transition frequency near 3.47 GHz. The microwave pulses are generated by a tunable source referenced to a stable Rubidium clock. As trap ellipticity increases (Fig. 2a), the degeneracy of the two upper sublevels is lifted. At an ellipticity near χ_m the state with no differential light shift emerges. An example of the $N = 0$ to $N = 1$ microwave spectrum in an elliptical trap is shown in Fig. 2b.

To find the precise QWP angle that achieves magic ellipticity, we scan the microwave frequency over the transition with a 10 μs π-pulse at varying trap depths and record the resonance frequencies (Fig. 2c). As expected, the slope of the resonance frequency as a function of QWP rotation is steeper at higher trap depths. The differential light shift is zero where the rotation angle dependence for different trap depths intersect. We de-
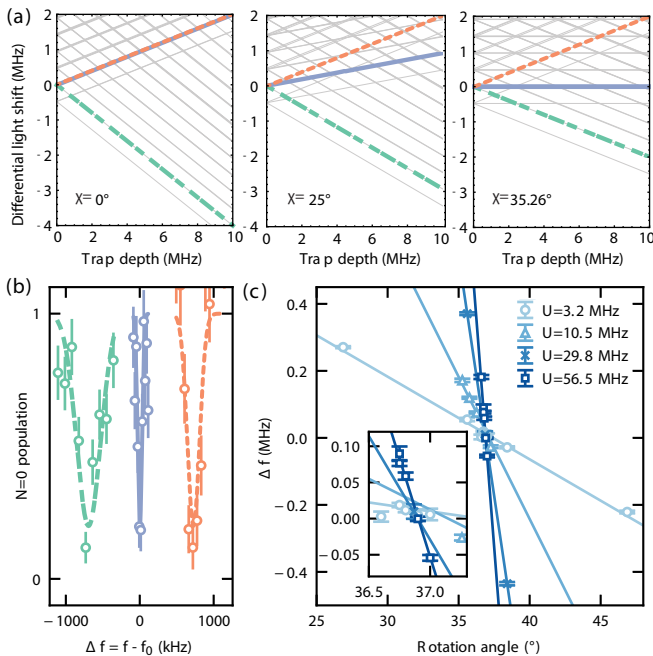
FIG. 3. Variations in rotational transition frequency across the 8 traps at two different trap depths U, and trap geometries and spacing. At a high trap depth of 41.2 MHz (red triangles) the transition frequency spans a range of 23 kHz across the array and at a lower depth of 1.34 MHz (blue circles) it spans < 1 kHz.

FIG. 2. $N = 0$ to $N = 1$ rotational transition in the rovibrational ground state of NaCs. (a) Differential light shift as a function of $N = 0$ trap depth at three distinct trap ellipticities. The colored red, blue, and green lines correspond to the light shifts of $N = 1, m_N$ sublevels of the hyperfine state $|3/2, 3/2, 7/2, 5/2\rangle$, and the grey lines correspond to the same for other hyperfine states. (b) An example of a measured rotational spectrum in the magic elliptically polarized trap. (c) Extracted resonant frequencies of the middle state from the rotational spectroscopy at different trap depths (U) and QWP rotational angles. The solid lines are linear fits.

termine the angle of the intersection with a weighted fit to be $36.83(10)°$, which deviates from the theoretically expected magic ellipticity angle by $\sim 1.6°$ [27]. The discrepancy may be due to birefringence of the glass cell assembly and the microscope objective. Nulling the differential lights shift allows a determination of the $N = 0$ to $N = 1$ transition frequency $f_0 = 3.4713203(7)$ GHz, taken as the transition frequency at the optimal ellipticity at trap depth $U =1.34$ MHz (see [27] for trap depth calibration) and is consistent with the low-depth regime measurement of the transition in Ref. [36].

Residual light shift at the optimal QWP angle reveal site-to-site variations in frequency across the 8 trap sites. To characterize these effects, we use a 60 μs microwave pulse to drive the rotational transition at a large trap depth of 41.2 MHz that magnifies light shifts. We find a site-to-site variation spanning 23 kHz (Fig. 3) with a 5(2) kHz average shift from the measured f_0, which constitutes a light shift to trap depth ratio of $1.2(5) \cdot 10^{-4}$. Despite the variation, this corresponds to a reduction in sensitivity by three orders of magnitude compared to the linearly polarized trap. The trap intensities across the array are made uniform to within 1%, such that they
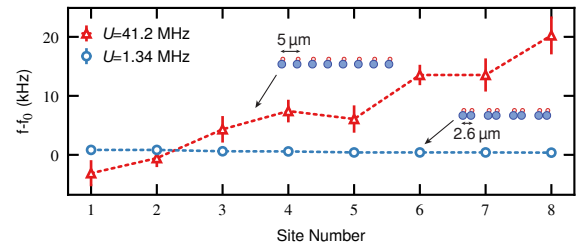
do not significantly contribute. We attribute the residual shifts to an ellipticity variation of $0.062°$ across the array. For the aspects of polarization ellipticity and intensity considered here, we expect negligible decoherence when a spin-echo pulse removes static frequency shifts.

With the reduced light shift sensitivity, $N = 0$ and $N = 1$ rotational superpositions exhibit long coherence that we characterize via Ramsey spectroscopy. Although the ensemble-averaged contrast would decay rapidly due to static light shift variation across the traps [27], a spin-echo π-pulse eliminates such dephasing. For a linearly polarized trap ($U = 1.0$ MHz), the $1/e$ decay time is $\tau = 0.57(2)$ ms, in agreement with a simulated coherence decay that incorporates measured intensity noise and the strong light shift sensitivity (Fig. 4a black line) [27]. With optimal ellipticity, the spin-echo coherence is extended by two orders of magnitude to 62(3) ms (blue circles in Fig. 4a). This coherence is further extended to 250(40) ms by use of repeated XY-8 sequences (up to 72 total pulses) [38, 39]. Figure 4b shows that the observed spin-echo coherence contrast depends sensitively on small changes of the QWP angle in the vicinity of magic ellipticity. The spin-echo contrast for individual traps at a precession time of 50 ms (Fig. 4c) shows a small amount of dephasing between sites. An overall phase shift of $73(3)°$ at long times (despite spin-echo) indicates a changing global frequency whose source is uncertain.

The effects of global intensity noise were simulated and do not account for observed decoherence [27]. Magnetic field fluctuation is also unlikely to be the cause, as the transition sensitivity is below 1 Hz/G while the field noise amplitude is 10^{-3} G. However, electric fields of 0.5 V/m with fluctuations of 0.012 V/m were measured in a similar vacuum glass cell environment [40]. Due to the large electric dipole moment of NaCs (4.6 Debye) and its easily polarizable nature, the quadratic Stark shift at such a field would cause frequency fluctuation of up to 12.6 Hz, which may explain the decoherence (see [27] for a Monte Carlo simulation).

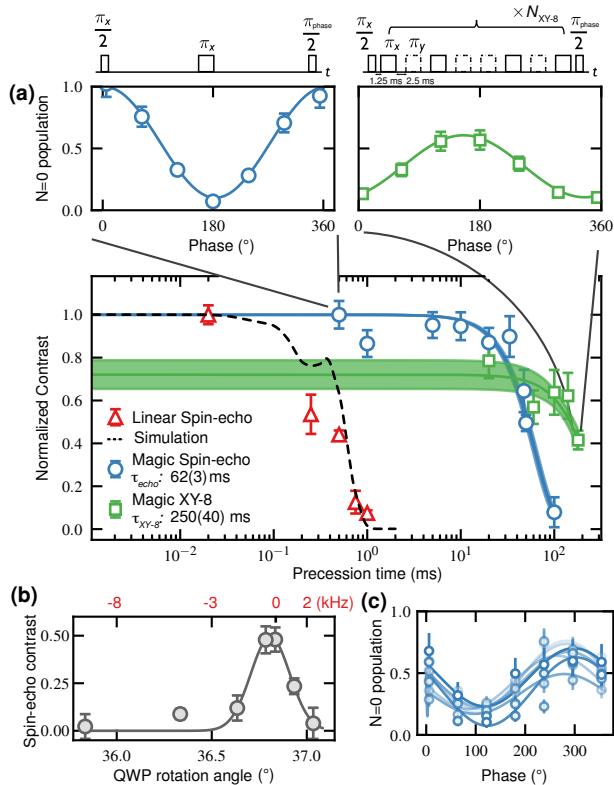Beyond single-body decoherence, a natural question is

FIG. 4. Rotational coherence times for approximately 1.3 MHz trap depth. (a) The coherence time is characterized using spin-echo phase Ramsey pulse sequence (shown in top left) in linear and magic elliptically polarized traps. In the linear trap, the phase Ramsey contrasts as a function of the free precession time (red, triangle) agree well with the simulated coherence decay based on intensity noise (black dotted line). The spin-echo coherence time is extended by two orders of magnitude in the magic trap (blue circle), which can be further improved (green square) using the XY-8 pulse sequence illustrated in the top right. The solid lines represent the fit to a Gaussian model $C(t) = \exp[-(t/\tau)^2]$. For the XY-8 pulse sequence, the overall amplitude is an additional fit parameter [37]. For the spin echo data, all contrasts are normalized to the shortest time point. An example spin-echo and XY-8 phase Ramsey scans are shown in the top left and right insets, respectively. (b) Spin-echo phase Ramsey contrast at 50 ms as a function of the QWP rotation angle. A Gaussian fit yields an optimal rotation angle of 36.81(3) degrees. The top axis is the corresponding light shifts expected from the ellipticity angle deviation relative to f_0. (c) Site-by-site Ramsey contrasts at 50 ms showing a global phase shift of 73(3)°. The contrast is normalized to the averaged N=0 population.

whether dipolar interaction causes the observed decoherence. However, because the polarization ellipse determines the dipolar axis, the interaction is reduced to zero in the present geometry $\phi = \chi_m$, with molecule separation along $\mathbf{x}$ (Fig. 1). We verify this experimentally by dropping molecules from every other site to extend the distance of the neighboring molecules to 10 μm and observe no change in the coherence. In the future, a half-

wave plate will allow adjustment of the anisotropic dipolar interaction into a maximal head-to-tail configuration while maintaining the magic condition.

In conclusion, we have demonstrated magic elliptical polarization trapping of polar molecules in the deep trap regime. The method reduces the light shift sensitivity between particular sublevels of the lowest two rotational states by three orders of magnitude and achieves a spin-echo rotational coherence time of 62(3) ms. This exceeds the expected 2 ms duration of dipolar entangling gates by a factor 30 for 2.6 μm molecule spacing. Furthermore, at this spacing and low depth, resonant frequency variations between neighboring molecules are less than 100 Hz (see Fig. 3); thus, decoherence caused by detuning variation can be effectively eliminated by using XY-8 decoupling pulses. We note that a sub-millisecond gate can be achieved by moving the traps closer. Coherence, limited by slow drifts that potentially arise from electric field fluctuations, may be further extended by dynamical decoupling and apparatus improvements such as placing in-vacuum electrodes [39, 41]. Additional tunable control over molecular dipole orientation will bring coherent dipolar interaction between motional ground-state molecules in tweezers within reach, leveraging the rich properties of molecules to enable high-fidelity gates [8], simulation of exotic phases [42, 43], and state engineering [44].

Note added - A related work demonstrates "magic" wavelength trapping of polar molecules [45].

———————————————

* A.J.P. and L.R.B.P contributed equally to this work.
† Current affiliation: University of California, Berkeley
‡ ni@chemistry.harvard.edu

[1] J. W. Park, Z. Z. Yan, H. Loh, S. A. Will, and M. W. Zwierlein, Second-scale nuclear spin coherence time of ultracold ^{23}Na^{40}K molecules, Science **357**, 372 (2017).

[2] S. Burchesky, L. Anderegg, Y. Bao, S. S. Yu, E. Chae, W. Ketterle, K.-K. Ni, and J. M. Doyle, Rotational coherence times of polar molecules in optical tweezers, Phys. Rev. Lett. **127**, 123202 (2021).

[3] P. D. Gregory, J. A. Blackmore, S. L. Bromley, J. M. Hutson, and S. L. Cornish, Robust storage qubits in ultracold polar molecules, Nature Physics **17**, 1149 (2021).

[4] J. Lin, J. He, M. Jin, G. Chen, and D. Wang, Seconds-scale coherence on nuclear spin transitions of ultracold polar molecules in 3d optical lattices, Phys. Rev. Lett. **128**, 223201 (2022).

[5] B. Yan, S. A. Moses, B. Gadway, J. P. Covey, K. R. A. Hazzard, A. M. Rey, D. S. Jin, and J. Ye, Observation of dipolar spin-exchange interactions with lattice-confined polar molecules, Nature **501**, 521 (2013).

[6] L. Christakis, J. S. Rosenberg, R. Raj, S. Chi, A. Morn-

ingstar, D. A. Huse, Z. Z. Yan, and W. S. Bakr, Probing site-resolved correlations in a spin system of ultracold molecules, Nature **614** (2023).

[7] D. DeMille, Quantum computation with trapped polar molecules, Phys. Rev. Lett. **88**, 067901 (2002).

[8] K.-K. Ni, T. Rosenband, and D. D. Grimes, Dipolar exchange quantum logic gate with polar molecules, Chemical Science **9**, 6830 (2018).

[9] C. M. Holland, Y. Lu, and L. W. Cheuk, On-Demand Entanglement of Molecules in a Reconfigurable Optical Tweezer Array (2022), arXiv:2210.06309.

[10] Y. Bao, S. S. Yu, L. Anderegg, E. Chae, W. Ketterle, K.-K. Ni, and J. M. Doyle, Dipolar spin-exchange and entanglement between molecules in an optical tweezer array (2022), arXiv:2211.09780.

[11] W. B. Cairncross, J. T. Zhang, L. R. B. Picard, Y. Yu, K. Wang, and K.-K. Ni, Assembly of a rovibrational ground state molecule in an optical tweezer, Physical Review Letters **126**, 123402 (2021).

[12] J. T. Zhang, L. R. B. Picard, W. B. Cairncross, K. Wang, Y. Yu, F. Fang, and K.-K. Ni, An optical tweezer array of ground-state polar molecules, Quantum Science and Technology **7**, 035006 (2022).

[13] D. K. Ruttley, A. Guttridge, S. Spence, R. C. Bird, C. R. L. Sueur, J. M. Hutson, and S. L. Cornish, Formation of ultracold molecules by merging optical tweezers (2023), arXiv:2302.07296 [physics.atom-ph].

[14] S. Kotochigova and D. DeMille, Electric-field-dependent dynamic polarizability and state-insensitive conditions for optical trapping of diatomic polar molecules, Phys. Rev. A **82**, 063421 (2010).

[15] B. Neyenhuis, B. Yan, S. A. Moses, J. P. Covey, A. Chotia, A. Petrov, S. Kotochigova, J. Ye, and D. S. Jin, Anisotropic polarizability of ultracold polar $^{40}K^{87}Rb$ molecules, Phys. Rev. Lett. **109**, 230403 (2012).

[16] F. Seeßelberg, X.-Y. Luo, M. Li, R. Bause, S. Kotochigova, I. Bloch, and C. Gohle, Extending rotational coherence of interacting polar molecules in a spin-decoupled magic trap, Phys. Rev. Lett. **121**, 253401 (2018).

[17] J. A. Blackmore, R. Sawant, P. D. Gregory, S. L. Bromley, J. Aldegunde, J. M. Hutson, and S. L. Cornish, Controlling the ac Stark effect of RbCs with dc electric and magnetic fields, Physical Review A **102**, 053316 (2020).

[18] R. Bause, M. Li, A. Schindewolf, X.-Y. Chen, M. Duda, S. Kotochigova, I. Bloch, and X.-Y. Luo, Tune-out and magic wavelengths for ground-state $^{23}Na^{40}K$ molecules, Phys. Rev. Lett. **125**, 023201 (2020).

[19] Q. Guan, S. L. Cornish, and S. Kotochigova, Magic conditions for multiple rotational states of bialkali molecules in optical lattices, Phys. Rev. A **103**, 043311 (2021).

[20] S. S. Kondov, C.-H. Lee, K. H. Leung, C. Liedl, I. Majewska, R. Moszynski, and T. Zelevinsky, Molecular lattice clock with long vibrational coherence, Nature Physics **15**, 1118 (2019).

[21] J. A. Blackmore, P. D. Gregory, S. L. Bromley, and S. L. Cornish, Coherent manipulation of the internal state of ultracold 87Rb133Cs molecules with multiple microwave fields, Physical Chemistry Chemical Physics 10.1039/D0CP04651E (2020).

[22] T. Rosenband, D. D. Grimes, and K.-K. Ni, Elliptical polarization for molecular stark shift compensation in deep optical traps, Opt. Express **26**, 19821 (2018).

[23] A. V. Taichenachev, V. I. Yudin, V. D. Ovsiannikov, and V. G. Pal'chikov, Optical lattice polarization effects on hyperpolarizability of atomic clock transitions, Phys. Rev. Lett. **97**, 173601 (2006).

[24] H. Kim, H. S. Han, and D. Cho, Magic polarization for optical trapping of atoms without stark-induced dephasing, Phys. Rev. Lett. **111**, 243004 (2013).

[25] A. Cooper, J. P. Covey, I. S. Madjarov, S. G. Porsev, M. S. Safronova, and M. Endres, Alkaline-earth atoms in optical tweezers, Phys. Rev. X **8**, 041055 (2018).

[26] J. Trautmann, D. Yankelev, V. Klüsener, A. J. Park, I. Bloch, and S. Blatt, $^1S_0-^3P_2$ magnetic quadrupole transition in neutral strontium, Phys. Rev. Res. **5**, 013219 (2023).

[27] See Supplemental Material, which includes Refs. [35, 40, 46–50], .

[28] M. Born and E. Wolf, *Principles of Optics, 6th ed.* (Cambridge University Press, 1980).

[29] J. T. Zhang, Y. Yu, W. B. Cairncross, K. Wang, L. R. Picard, J. D. Hood, Y.-W. Lin, J. M. Hutson, and K.-K. Ni, Forming a Single Molecule by Magnetoassociation in an Optical Tweezer, Physical Review Letters **124**, 253401 (2020).

[30] M. Endres, H. Bernien, A. Keesling, H. Levine, E. R. Anschuetz, A. Krajenbrink, C. Senko, V. Vuletic, M. Greiner, and M. D. Lukin, Atom-by-atom assembly of defect-free one-dimensional cold atom arrays, Science **354**, 1024 (2016).

[31] D. Barredo, S. de Léséleuc, V. Lienhard, T. Lahaye, and A. Browaeys, An atom-by-atom assembler of defect-free arbitrary two-dimensional atomic arrays, Science **354**, 1021 (2016).

[32] Y. Yu, N. R. Hutzler, J. T. Zhang, L. R. Liu, J. D. Hood, T. Rosenband, and K.-K. Ni, Motional-ground-state cooling outside the Lamb-Dicke regime, Physical Review A **97**, 063423 (2018).

[33] L. R. Liu, J. D. Hood, Y. Yu, J. T. Zhang, K. Wang, Y.-W. Lin, T. Rosenband, and K.-K. Ni, Molecular Assembly of Ground-State Cooled Single Atoms, Physical Review X **9**, 021039 (2019).

[34] L. R. B. Picard, J. T. Zhang, W. B. Cairncross, K. Wang, G. E. Patenotte, A. J. Park, Y. Yu, L. R. Liu, J. D. Hood, R. González-Férez, and K.-K. Ni, High resolution photoassociation spectroscopy of the excited $c^3\Sigma_1^+$ potential of $^{23}Na^{133}Cs$, Phys. Rev. Res. **5**, 023149 (2023).

[35] J. T. Zhang, *Assembling an array of polar molecules with full quantum-state control*, Ph.D Thesis, Harvard University (2021).

[36] N. Bigagli, C. Warner, W. Yuan, S. Zhang, I. Stevenson, T. Karman, and S. Will, Collisionally stable gas of bosonic dipolar ground state molecules (2023), arXiv:2303.16845 [cond-mat.quant-gas].

[37] The overall amplitude was left as a fit parameter to account for the off-resonant coupling to $N=1$ non-magic states.

[38] T. Gullion, D. B. Baker, and M. S. Conradi, New, compensated carr-purcell sequences, Journal of Magnetic Resonance (1969) **89**, 479 (1990).

[39] J.-R. Li, K. Matsuda, C. Miller, A. N. Carroll, W. G. Tobias, J. S. Higgins, and J. Ye, Tunable itinerant spin dynamics with polar molecules, Nature **614**, 70 (2023).

[40] P. L. Ocola, I. Dimitrova, B. Grinkemeyer, E. Guardado-Sanchez, T. Dordevic, P. Samutpraphoot, V. Vuletic, and M. D. Lukin, Control and entanglement of individual rydberg atoms near a nanoscale device (2022),

arXiv:2210.12879 [physics.atom-ph].

[41] J. T. Wilson, S. Saskin, Y. Meng, S. Ma, R. Dilip, A. P. Burgers, and J. D. Thompson, Trapping alkaline earth rydberg atoms optical tweezer arrays, Phys. Rev. Lett. **128**, 033201 (2022).

[42] N. Y. Yao, M. P. Zaletel, D. M. Stamper-Kurn, and A. Vishwanath, A quantum dipolar spin liquid, Nature Physics **14**, 405 (2018).

[43] L. Homeier, T. J. Harris, T. Blatz, U. Schollwöck, F. Grusdt, and A. Bohrdt, Antiferromagnetic bosonic t-j models and their quantum simulation in tweezer arrays (2023), arXiv:2305.02322 [cond-mat.quant-gas].

[44] B. Sundar, B. Gadway, and K. R. A. Hazzard, Synthetic dimensions in ultracold polar molecules, Scientific Reports **8**, 3422 (2018).

[45] P. D. Gregory, L. M. Fernley, A. L. Tao, S. L. Bromley, J. Stepp, Z. Zhang, S. Kotochigova, K. R. A. Hazzard, and S. L. Cornish, Second-scale rotational coherence and dipolar interactions in a gas of ultracold polar molecules (2023), arXiv:2306.02991 [physics.atom-ph].

[46] R. Grimm, M. Weidemüller, and Y. B. Ovchinnikov, Advances in atomic, molecular, and optical physics (2000) Chap. Optical dipole traps for neutral atoms, pp. 95–170.

[47] R. Vexiau, D. Borsalino, M. Lepers, A. Orban, M. Aymar, O. Dulieu, and N. Bouloufa-Maafa, Dynamic dipole polarizabilities of heteronuclear alkali dimers: optical response, trapping and control of ultracold molecules, International Reviews in Physical Chemistry **36**, 709 (2017).

[48] J. Aldegunde, H. Ran, and J. Hutson, Manipulating ultracold polar molecules with microwave radiation: The influence of hyperfine structure, Physical Review A **80**, 043410 (2009).

[49] P. Cappellaro, *Quantum Theory of Radiation—MIT Course No. 22.51* (Cambridge MA, 2012) MIT OpenCourseWare.

[50] B. Chen and J. Pu, Tight focusing of elliptically polarized vortex beams, Applied Optics **48**, 1288 (2009).